The Plant Cell, Vol. 21: 3119–3132, October 2009, www.plantcell.org

Phenotypic Plasticity of Adventitious Rooting in *Arabidopsis* Is Controlled by Complex Regulation of AUXIN RESPONSE FACTOR Transcripts and MicroRNA Abundance [W]

Laurent Gutierrez,[a,b] John D. Bussell,[a,c] Daniel I. Păcurar,[a,d] Josèli Schwambach,[a,1] Monica Păcurar,[a,d] and Catherine Bellini[a,e,2,3]

[a] Umeå Plant Science Centre, Department of Forest Genetics and Plant Physiology, Swedish University of Agricultural Sciences, SE-90183 Umeå, Sweden

[b] Centre de Ressources Régionales en Biologie Moléculaire, Université de Picardie Jules Verne, 80039 Amiens, France

[c] Australian Research Council Centre of Excellence in Plant Energy Biology, University of Western Australia, Crawley WA 6009, Australia

[d] University of Agricultural Sciences and Veterinary Medicine, 400372 Cluj Napoca, Romania

[e] Institut Jean-Pierre Bourgin, Unité de Recherche 501, Institut National de la Recherche Agronomique Centre de Versailles, 78026 Versailles Cedex, France

The development of shoot-borne roots, or adventitious roots, is indispensable for mass propagation of elite genotypes. It is a complex genetic trait with a high phenotypic plasticity due to multiple endogenous and environmental regulatory factors. We demonstrate here that a subtle balance of activator and repressor *AUXIN RESPONSE FACTOR* (*ARF*) transcripts controls adventitious root initiation. Moreover, microRNA activity appears to be required for fine-tuning of this process. Thus, *ARF17*, a target of *miR160*, is a negative regulator, and *ARF6* and *ARF8*, targets of *miR167*, are positive regulators of adventitious rooting. The three *ARF*s display overlapping expression domains, interact genetically, and regulate each other's expression at both transcriptional and posttranscriptional levels by modulating *miR160* and *miR167* availability. This complex regulatory network includes an unexpected feedback regulation of microRNA homeostasis by direct and nondirect target transcription factors. These results provide evidence of microRNA control of phenotypic variability and are a significant step forward in understanding the molecular mechanisms regulating adventitious rooting.

INTRODUCTION

The regulation of gene expression through the microRNA (miRNA) pathway is a relatively new discovery. In the last 10 years, rapid progress has led to the identification of genes involved in the processing and maturation of miRNAs (Voinnet, 2009). However, mechanisms for regulation of their production and for the maintenance of their homeostasis are still unclear in both plants and animals. miRNAs are required for fine-tuning of gene expression for adaptation to subtle endogenous (e.g., hormonal) or environmental fluctuations. Phenotypic variability associated with complex genetic traits is one of the manifestations of these variations in gene expression. The activity of miRNAs is suspected to be instrumental for phenotypic variability, although it has not been clearly demonstrated. Interestingly, the fact that the regulation of *ARF8* by *miR167* was recently shown to be a determinant for lateral root plasticity in response to nitrogen (Gifford et al., 2008) supports this hypothesis.

We are interested in dissecting the genetic and molecular mechanisms that regulate the development of shoot-borne roots, also called adventitious roots, using the model plant *Arabidopsis thaliana*. Adventitious rooting is a heritable quantitative trait that is affected by multiple endogenous and environmental factors. One of the endogenous factors long known to play a key role in the control of adventitious rooting is auxin, but our knowledge of the molecular mechanisms involved is rudimentary. However, disruption of the auxin-inducible *CROWN ROOTLESS1/ADVENTITIOUS ROOTLESS1* (*CRL1/ARL1*) gene, which encodes a member of the plant-specific LOB protein family, has been shown to prevent initiation of adventitious crown root primordia in rice (*Oryza sativa*; Inukai et al., 2005; Liu et al., 2005). The promoter of the *CRL1/ARL1* gene contains specific *cis*-regulatory elements that interact with a rice transcription factor from the auxin response factor (ARF) family (Inukai et al., 2005). Our previous characterization of *argonaute1* and *superroot 2* single and double mutants in *Arabidopsis* allowed us to identify several genes potentially involved in the regulation of adventitious rooting (Sorin et al., 2005, 2006). We showed that a transgenic *Arabidopsis* line overexpressing the *ARF17* gene developed fewer adventitious roots than wild-type plants, confirming the potential role of *ARF* genes in the regulation of adventitious root development by auxin (Sorin et al., 2005).

[1] Current address: Departamento de Botânica, Universidade Federal do Rio Grande do Sul, 91509-900, Porto Alegre, Rio Grande do Sul, Brazil.
[2] Current address: Department of Plant Physiology, Umeå University, SE-90187 Umeå, Sweden.
[3] Address correspondence to catherine.bellini@plantphys.umu.se.
The author responsible for distribution of materials integral to the findings presented in this article in accordance with the policy described in the Instructions for Authors (www.plantcell.org) is: Catherine Bellini (catherine.bellini@plantphys.umu.se).
[W] Online version contains Web-only data.
www.plantcell.org/cgi/doi/10.1105/tpc.108.064758

ARF transcription factors relay auxin signaling at the transcriptional level by regulating the expression of auxin-responsive genes (Guilfoyle and Hagen, 2007). The transcript abundance of eight out of the 23 *Arabidopsis ARFs* is regulated by miRNAs (Rhoades et al., 2002; Mallory et al., 2005; Wu et al., 2006) and *trans*-acting small interfering RNAs (Allen et al., 2005; Williams et al., 2005). *ARF6* and *8* are targets for *miR167*, while *ARF10*, *16*, and *17* are targets for *miR160*.

Previously, we showed that *ARF17* (At1g77850) was a negative regulator of adventitious rooting that could potentially integrate auxin and light signaling pathways affecting this process (Sorin et al., 2005). In this contribution, we demonstrate that the auxin response factors *ARF6* (At1g30330) and *ARF8* (At5g37020) are positive regulators of adventitious root formation. Furthermore, we show that the expression of these three ARFs is regulated by light and that they act in a complex regulatory network that includes feedback regulatory loops controlling the abundance of their respective regulatory miRNAs, thereby modulating the balance between positive and negative regulators of adventitious rooting.

RESULTS

ARF6, *ARF8*, and *ARF17* Regulate Adventitious Rooting

In order to assess the potential contributions of different miRNA-targeted *ARF* genes to the regulation of adventitious rooting, we analyzed adventitious root formation in *arf6*, *arf8*, *arf10*, and *arf16* knockout (KO) mutants and *ARF6*, *8*, and *17* overexpressing (OX) lines under previously described conditions (Sorin et al., 2005). Seeds were stratified for 48 h and then seedlings etiolated for ~48 h (Figure 1A) before transfer to light and counting of adventitious roots after 7 d in the light (Figure 1B). The average numbers of adventitious roots developed by *arf10-3*, *arf10-4*, and *arf16-3* single mutants and double *arf10-3 arf16-3* mutants did not significantly differ from the average number developed by wild-type counterparts (Figure 1C), suggesting that *ARF10* and *16* (At2g28350 and At4g30080) do not play a significant role in adventitious rooting, either singly or in combination. By contrast, *arf6-3*, *arf8-1*, *arf8-7*, and *ARF17-OX* plants produced fewer adventitious roots than wild-type plants, while *ARF6-OX* and *ARF8-OX* plants developed more (Figure 1C). Since no *ARF17* knockout mutant was available, we analyzed lines overexpressing *MIR160a* (At2g39175) and *MIR160c* (At5g46845) genes (*miR160a-OX* and *miR160c-OX*, respectively), in which the accumulation of *miR160* specifically targets *ARF10*, *ARF16*, and *ARF17* transcripts for degradation (Wang et al., 2005). Since the *arf10-3 arf16-3* double knockout mutant showed no apparent defect in adventitious rooting, the increased frequencies of adventitious roots observed in *MIR160a-OX* and *MIR160c-OX* mutants were presumably solely due to the increased degradation of *ARF17* transcripts. When *ARF17* is overexpressed in knockout *arf6-3* and *arf8-7* mutant backgrounds, fewer adventitious roots than in *ARF17* overexpressing lines or *arf6-3* and *arf8-7* single mutants were observed (Figure 1C), indicating an additive effect due to the overexpression of a negative regulator in mutants lacking a positive regulator of adventitious rooting. In our growth conditions, no significant differences in the length or number of lateral roots were observed between any of the mutant and overexpressing lines (Figure 1D; see Supplemental Figures 1A and 1B online). Taken together, our findings demonstrate a role for the *ARF6* and *ARF8* genes as positive regulators of adventitious rooting and substantiate our previous finding that *ARF17* negatively regulates this process.

Light Regulation of *ARF6*, *8*, and *17* during Adventitious Root Initiation

We next characterized the expression of *ARF6*, *ARF8*, and *ARF17* and their respective regulatory miRNAs (*miR167* and *miR160*) during the early steps of adventitious root formation using transcriptional fusions constructs containing β-glucuronidase (GUS) fused to the respective promoters (Sorin et al., 2005). At time T0 (i.e., etiolated seedlings prior to transfer to the light [as in Figure 1A]), *promMIR160c:GUS* was strongly and constitutively expressed in the entire seedling (Figure 2A). This expression pattern was maintained whether the seedlings were kept in the dark for additional 48 (T48D) or 72 h (T72D) (Figures 2B and 2C) or incubated under the light for 48 (T48L) or 72 h (T72L) (Figures 2D and 2E). Similarly we analyzed the expression of *promMIR167a:GUS*, *promMIR167b:GUS*, *promMIR167c:GUS*, and *promMIR167d:GUS* in the same conditions and showed that the four promoters displayed slightly different expression patterns, but no difference was observed between dark- and light-grown seedlings (Figures 2A to 2E). These results suggest that light has no effect on the regulation of the expression of *MIR160*c (At5g46845) and *MIR167a*, *b*, *c*, and *d* (At3g22886, At3g63375, At3g04765, and At1g31173, respectively) genes. In order to confirm that the GUS staining correlates with the presence of the mature miRNAs *miR160* and *miR167a*, *b*, *c*, and *d*, we quantified these transcripts in the different organs of seedlings at T72L, using real-time RT-PCR (see Supplemental Figure 2A online). In accordance with the GUS staining, *miR160* was indeed found to be highly expressed in all the different organs of the seedlings, while the organ-specific patterns were confirmed for *miR167a* to *d* (Figure 2O).

At time T0, *promARF6:GUS* and *promARF8:GUS* were expressed in the upper tier of the hypocotyl, the hypocotyl-root junction and the root tip, whereas *promARF17:GUS* was strongly expressed in the cotyledons, the upper tier of the hypocotyls, and the hypocotyl-root junction (Figure 2F). At T0, *promARF6:GUS* expression, unlike that of *promARF8:GUS* and *promARF17:GUS*, was also detected in the vascular region of both the hypocotyls and roots. At T48D and T72D, a reduction of the intensity of the GUS staining was observed for *promARF6:GUS* and *promARF8:GUS*, whereas that with *promARF17:GUS* remained unchanged (Figures 2G and 2H) relative to T0. By contrast, 48 h after transfer to the light, expression of *promARF8:GUS* increased in the hypocotyl (Figure 2I), and at T72L significant shifts had occurred; *promARF6:GUS* expression had increased in all organs and *promARF8:GUS* expression had increased in roots and the hypocotyl but was still very weak in the cotyledons. Expression of *promARF17:GUS* had decreased, becoming only very weakly detectable in the root and hypocotyl vascular region and greatly reduced in the cotyledons (Figure 2J).

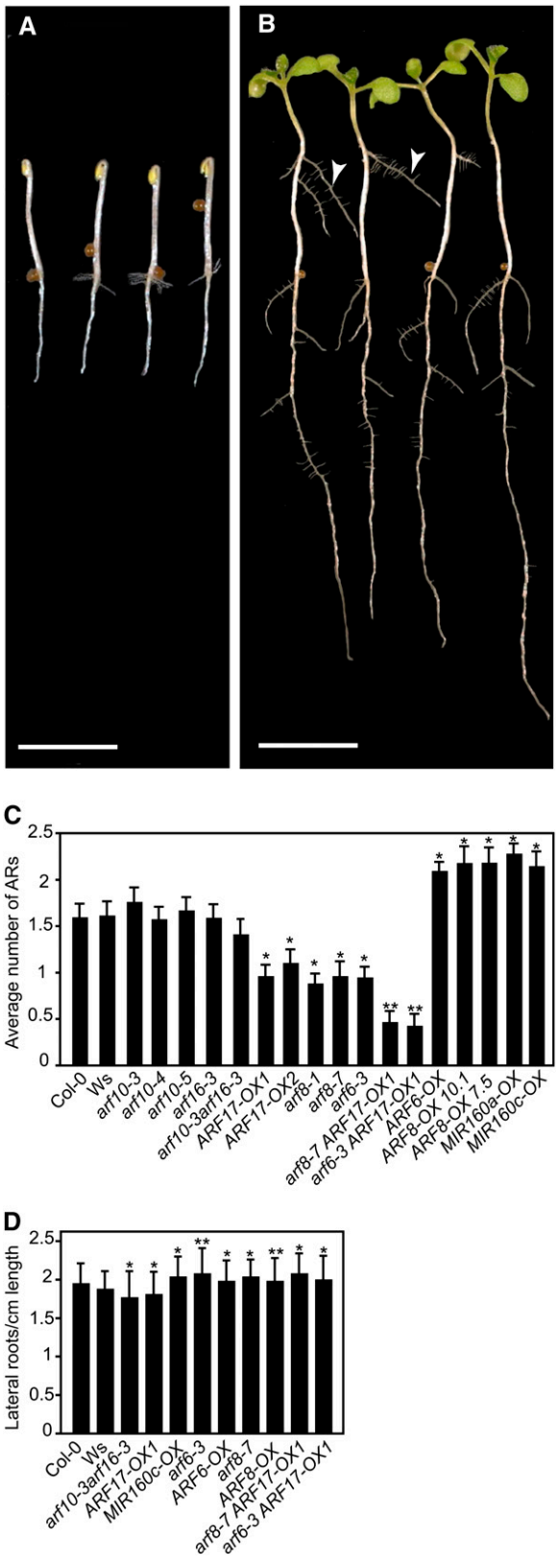

Figure 1. *ARF6*, *ARF8*, and *ARF17* Regulate Adventitious Root Development.

After transfer to the light, *promARF6:GUS* and *promARF8:GUS* expression was homogeneously detected in the vascular tissue of the hypocotyl, accompanied by increased frequencies of adventitious root primordia initials and developing primordia (e.g., Figure 2K). Close-up views of young adventitious root primordia after 72 h in light revealed that *promARF6:GUS* (Figure 2L) and *promARF8:GUS* (Figure 2M) were highly expressed in the adventitious root primordia, as were *promMIR167a:GUS* and *promMIR167c:GUS* (Figure 2E), whereas *promARF17:GUS* expression was restricted to the vascular cells close to the primordia (Figure 2N).

In order to confirm that the expression profile observed with the *prom:GUS* fusions correlated with the presence of a transcript, we analyzed by real-time RT-PCR the steady state levels of total (T) and uncleaved (UC) *ARF* transcripts in the different organs (cotyledons, hypocotyls, and root) of seedlings at T0 and T72L (Figures 2P to 2S). Here, the uncleaved transcript level refers to the amount of steady state mRNA detectable using primers bounding the transcripts' miRNA sites, while the total transcript level refers to the amount of transcript detectable using primers corresponding to parts of the 3′ region of the mRNA (see Supplemental Figure 2B online). The latter includes both cleaved and uncleaved products, although it may not reflect the absolute transcription level since the *ARF* transcripts may be subject to other degradation mechanisms in addition to their cleavage through the miRNA pathway. The amount of total and uncleaved transcript matched the GUS pattern observed in all the organs at both T0 and T72L. *ARF6-UC* (and *ARF6-T*) was greatly elevated at T72L compared with T0 in the root, hypocotyls, and cotyledons (Figures 2P to 2R). This mirrored the *promARF6:GUS* result where GUS staining was increased in all organs at T72L versus T0 (Figures 2F and 2J). Similar results were

(A) Dark grown wild-type seedlings. Hypocotyls have reached 6 mm. Bar = 5 mm.

(B) Wild-type seedlings 7 d after transfer to the light. Arrows indicate adventitious roots on the hypocotyls. Bar = 5 mm.

(C) Adventitious roots were counted in seedlings that were first etiolated in the dark, until their hypocotyls were 6 mm long, and then transferred to the light for 7 d. Data from three independent biological replicates, each of at least 30 seedlings, were pooled and averaged. Error bars indicate ± SE. A one-way analysis of variance (ANOVA) combined with the Tukey's multiple comparison test indicated that the values marked with one asterisk were significantly different from wild-type values and those marked with two asterisks were significantly different from values obtained from single mutants or ARF17-OX lines ($P < 0.01$; $n > 90$).

(D) The lateral roots of the same seedlings were counted, and the lengths of their main roots were measured. No significant differences in either the length or number of lateral roots were observed between any of the lines (see Supplemental Figures 1A and 1B online). For simplicity, we show the mean lateral root density, expressed as the number of lateral roots divided by the length of the main root, of at least 30 plants of each line described in Methods. The experiments were repeated three times. Error bars indicate ± SE. A one-way ANOVA combined with the Tukey's multiple comparison test indicated that the values marked with one asterisk were not significantly different from wild-type (Columbia-0 [Col-0]) values ($P = 0.99$; $n > 45$) and those marked with two asterisks were not significantly different from wild-type (Wassilewskija [Ws]) values ($P = 0.88$; $n > 45$).

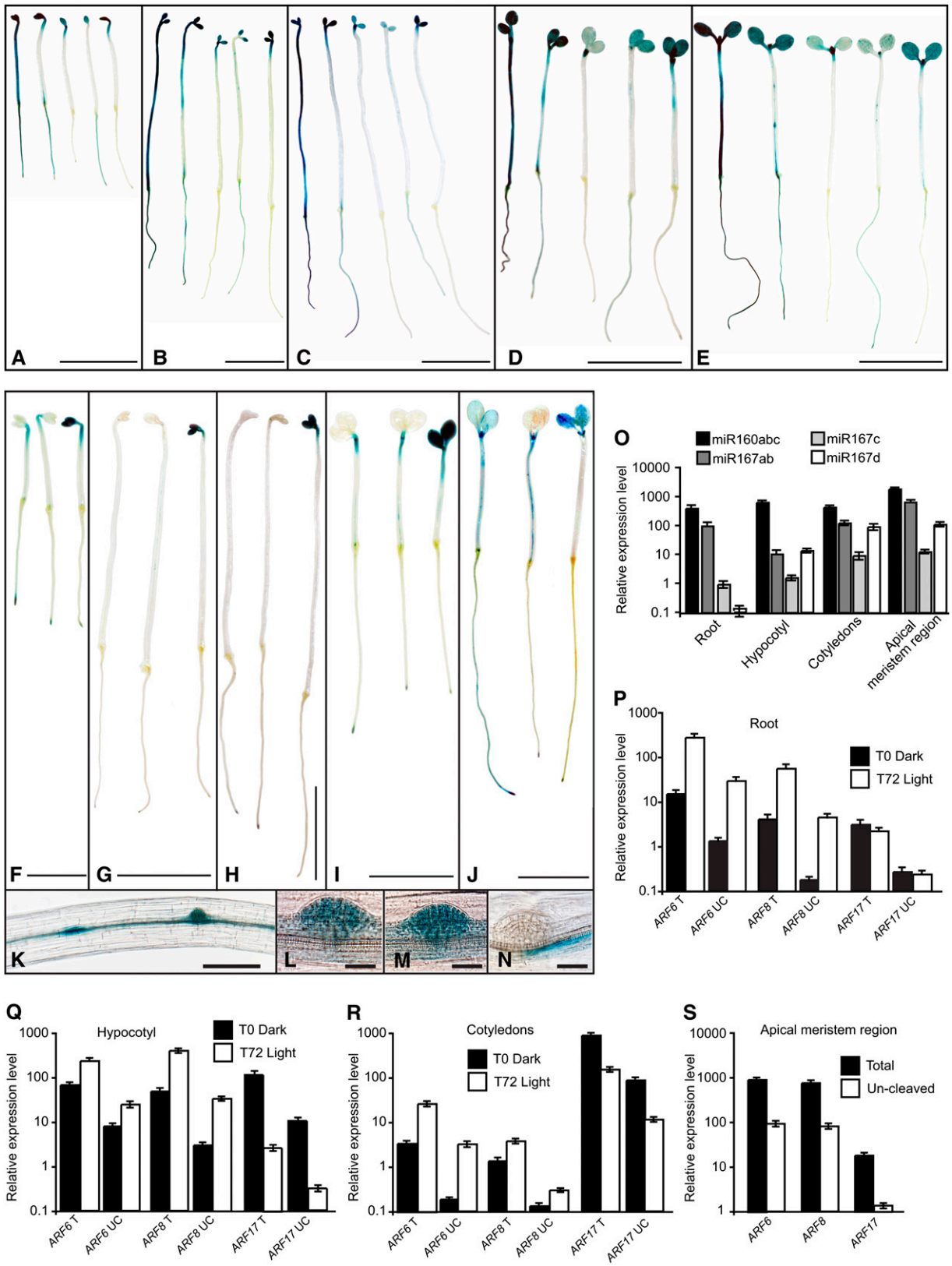

Figure 2. Expression Patterns of *MIR160c*, *MIR167a*, *MIR167b*, *MIR167c*, *MIR167d*, *ARF6*, *ARF8*, and *ARF17* during the Early Stages of Adventitious Root Formation.

observed for *ARF8-UC* (and *ARF8-T*). In addition, the weaker GUS expression for *promARF8:GUS* at T72L in the cotyledons and the root compared with that for *promARF6:GUS* (Figure 2J) reflects the lower level of *ARF8-UC* (and *ARF8-T*) transcripts (Figures 2P and 2R). At T0, in the hypocotyl, *ARF6* (T and UC), *ARF8* (T and UC), and *ARF17* (UC and T) transcripts were detected at similar levels (Figure 2Q) as suggested by the GUS staining in the hypocotyl (Figure 2F). Still in agreement with the GUS staining observed in the hypocotyl at T72L (Figure 2J), the levels of *ARF6* (T and UC) and *ARF8* (T and UC) mRNA were increased at T72L compared with their level at T0, whereas that of *ARF17* (UC and T) was decreased compared with its level at T0 (Figure 2Q). Similarly, the *ARF17* (UC and T) mRNA level was decreased in the cotyledons at T72L (Figure 2R), confirming the *promARF17:GUS* expression (Figures 2F and 2J). *ARF17*-UC and T mRNA level was also lower than that of ARF6 or ARF8 in the apical meristem region at T72 (Figure 2S). Altogether, these results confirm the positive effect of light on *ARF6* and *ARF8* expression and the negative effect of light on *ARF17* expression.

In an attempt to understand which light pathway could be involved in the regulation of *ARF6*, *ARF8*, and *ARF17* expression, we analyzed the expression pattern of *promARF6:GUS*, *promARF8:GUS*, and *promARF17:GUS* 72 h after transfer into monochromatic light conditions (see Supplemental Figure 3 online). At 72 h after transfer into blue light conditions (460 nm, 80 μmol m^{-2} s^{-1}, 24°C $\pm$ 2°C), a similar pattern to that observed 72 h after transfer to white light was observed (Figure 2J; see Supplemental Figure 3B online). Expression of *promARF17:GUS* was decreased in the hypocotyl and the cotyledons at T72 (see Supplemental Figure 3B online) compared with T0 (see Supplemental Figure 3A online), whereas an increase of the expression of *promARF6:GUS* and *promARF8:GUS* was observed in the hypocotyls and the root but not in the cotyledons (see Supplemental Figure 3B online). At T72 in red light (650 nm, 15 μmol m^{-2} s^{-1}, 22°C $\pm$ 2°C), expression of *promARF17:GUS* was decreased compared with T0 (see Supplemental Figure 3C online). GUS staining was observed with *promARF6:GUS* in the root and weakly in the hypocotyls, whereas *promARF8:GUS* expression was detected in the hypocotyls and to a lesser extent in the root (see Supplemental Figure 3C online). In far-red light (750 nm, 13 μmol m^{-2} s^{-1}, 23°C $\pm$ 2°C), no GUS expression was detected at T72 in the hypocotyl for *promARF8:GUS*, whereas it could be detected in the case of *promARF6:GUS* (see Supplemental Figure 3D online). As in blue and red light conditions, the expression of *promARF17:GUS* was reduced at T72 in far-red light compared with T0 (see Supplemental Figure 3D online). These preliminary results suggest that the regulation of *ARF6*, *ARF8*, and *ARF17* by light is complex and involves more than a single pathway. *promARF17:GUS* seems to respond in a similar way irrespective of the different light conditions. *promARF6:GUS* and *promARF8:GUS* respond similarly to each other under blue and red light, whereas a differential response to far-red light was observed, suggesting that specific mechanisms are involved in the regulation of the homeostasis of these three *ARF*s.

Control of Adventitious Rooting by Repressor and Activator *ARF*s

The observed mutant phenotypes and the combination of both overlapping and mutually exclusive expression profiles displayed by the three examined *ARF* genes suggested that the phenotypic variability could be due to shifts in the abundance of either activator or repressor *ARF*s. We therefore tested the possibility that cross-regulation occurs between these transcription factors during adventitious root formation by analyzing steady state levels of total and uncleaved *ARF* transcripts in the hypocotyls of overexpressing and knockout *ARF* lines by real-time RT-PCR (Figure 3). Differences in the level of uncleaved mRNA species provide indications of possible regulation of posttranscriptional degradation through the miRNA pathway (Thomson et al., 2006), whereas the total transcript levels reveal possible differences between mutant and wild-type lines in either transcriptional regulation or posttranscriptional regulation independent from the miRNA pathway. In each line, variations in the levels of total and uncleaved transcripts of all three *ARF*s were observed (Figure 3). Nevertheless, the mutants' ratios between

Figure 2. (continued).

(A) to **(E)** GUS staining of *promMIR160c:GUS*, *promMIR167a:GUS*, *promMIR167b:GUS*, *promMIR167c:GUS*, and *promMIR167d:GUS* (arranged from left to right in each panel) in seedlings grown in the dark until their hypocotyls were 6 mm long **(A)**, after an additional 48 h **(B)** and 72 h **(C)** in the dark or after transfer to the light for 48 h **(D)** and 72 h **(E)**.

(F) to **(J)** GUS staining of *promARF6:GUS*, *promARF8:GUS*, and *promARF17:GUS* (arranged from left to right in each panel) in seedlings grown in the dark until their hypocotyls were 6 mm long **(F)**, after an additional 48 h **(G)** and 72 h **(H)** in the dark, or 48 h **(I)** and 72 h **(J)** after their transfer to the light. Bars = 5 mm in **(A)** to **(J)**.

(K) Close-up image of *promARF6:GUS* hypocotyl from seedling shown in **(J)**.

(L) to **(N)** Close-up up images from the same seedlings as in **(J)**; young adventitious root primordia of *promARF6:GUS* **(L)**, *promARF8:GUS* **(M)**, and *promARF17:GUS* **(N)** plants after 72 h in the light. Bars = 0.5 mm in **(K)** and 50 μm in **(L)** to **(N)**.

(O) Quantification by real-time RT-PCR of the steady state level of miRNA species *miR160abc*, *miR167ab*, *miR167c*, and *miR167d* in the different organs (cotyledons, apical meristem, hypocotyls, and root) of wild-type seedlings etiolated and then transferred to the light for 72 h as in **(E)** and **(J)**.

(P) to **(R)** Quantification by real-time RT-PCR of *ARF6*, *ARF8*, and *ARF17* transcripts in roots **(P)**, hypocotyls **(Q)**, and cotyledons **(R)** of wild-type seedlings etiolated as in **(F)** (black bars) and after transfer to the light for 72 h as in **(J)** (white bars). T, total transcript; UC, uncleaved transcript.

(S) Confirmation by real-time RT-PCR of *ARF6*, *ARF8*, and *ARF17* transcripts in the apical meristem region from seedlings transferred to the light for 72 h as in **(J)**.

(O) to **(S)** Expression values are expressed relative to the expression level of *APT1* used as a reference gene as described in Methods.

Error bars indicate $\pm$ SE obtained from three independent RT-PCR experiments.

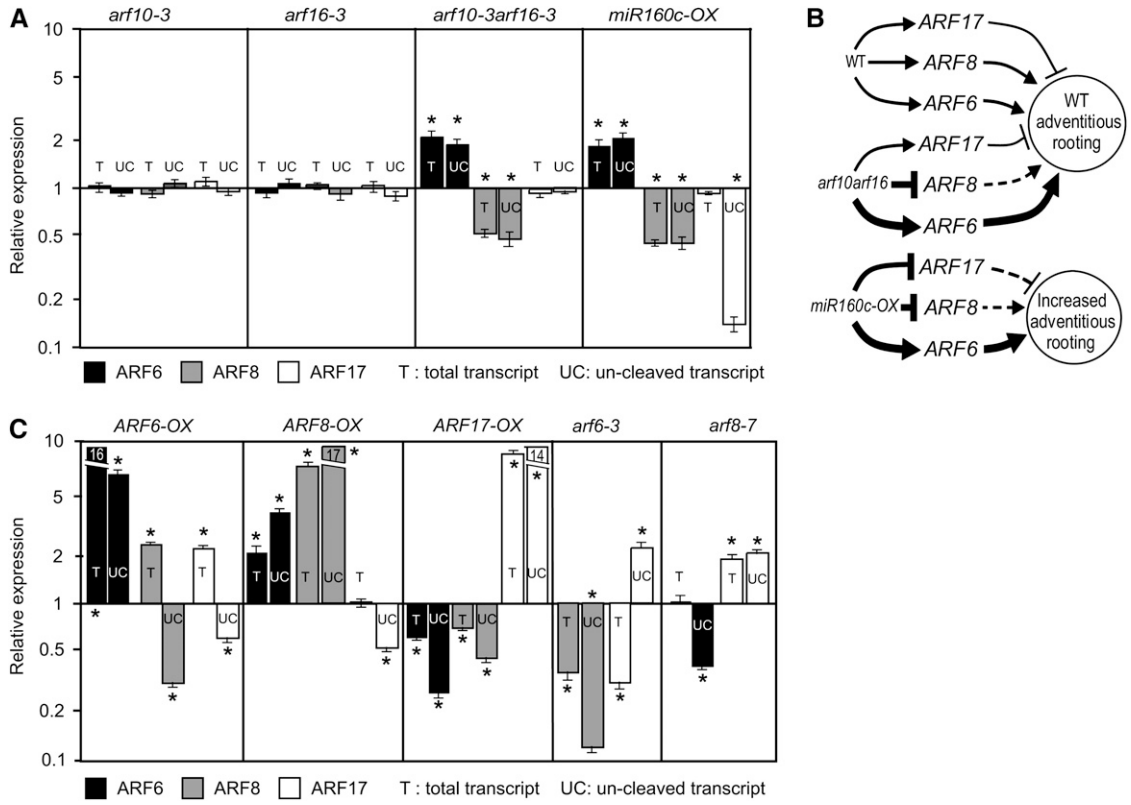

Figure 3. Quantification by Real-Time RT-PCR of *ARF6*, *ARF8*, and *ARF17* Transcripts in Hypocotyls of *ARF* Mutant Lines Reveals Regulatory Loops.

(A) and **(B)** Comparison of *ARF6*, *ARF8*, and *ARF17* transcript levels found in the *arf10-3* mutant, *arf16-3* mutant, *arf10-3 arf16-3* double KO, and *MIR160c-OX* line showing the importance of the balance between these transcript levels for control of adventitious rooting.

(C) Steady state levels of both the total (T) and uncleaved (UC) *ARF* transcripts were quantified in the hypocotyls of representative *ARF6-OX*, *ARF8-OX*, and *ARF17-OX* lines and *arf6-3* and *arf8-7* KO mutants.

Transcript abundance was quantified in the hypocotyls of representative *ARF* mutant or overexpressing lines etiolated and transferred to the light for 72 h. Gene expression values shown are relative to the expression in the wild type, for which the value is set to 1. Error bars indicate ± SE obtained from three independent RT-PCR experiments. A one-way ANOVA combined with the Dunnett's comparison test indicated that the values marked with an asterisk were significantly different from wild-type value ($P < 0.01$; $n = 3$). All quantifications were repeated using two additional independent biological replicates and gave similar results.

putative activators and inhibitors of adventitious rooting always correlated with their observed increases and reductions in frequencies of adventitious roots, relative to wild-type counterparts, respectively. This complex cross-regulation is described below.

Repressor/Activator Balance Is Unaltered by Disruptions to *ARF10* and *ARF16*

No significant deviations from the wild type in adventitious rooting parameters were observed in the *arf10-3* and *arf16-3* mutants, and we did not observe any modification of the expression of *ARF6*, *ARF8*, and *ARF17* genes in these single mutants (Figure 3A). Interestingly, however, although the *arf10-3 arf16-3* double mutant displayed no adventitious rooting phenotypic deviation from the wild type (Figure 1C), it accumulated higher levels of both *ARF6-T* and *ARF6-UC* transcripts, with simultaneous reductions in *ARF8-T* and *ARF8-UC* transcript levels, while those of *ARF17* remained unchanged. Since *ARF6* and *ARF8* are positive regulators of adventitious rooting, we suggest that the increase in *ARF6* expression is compensated for by the decrease in *ARF8* expression in these plants, in effect maintaining the balance between activators and repressors, and thus maintaining a wild-type phenotype (Figures 1C and 3A). The overexpression of *miR160c*, which targets *ARF10*, *ARF16*, and *ARF17* for degradation (Wang et al., 2005), has the same effect on *ARF6* and *ARF8* expression presumably due to the down-regulation of *ARF10* and *16* (Figure 3A). However, the large decrease in the level of *ARF17-UC* (Figure 3A) shifts the balance toward activators, leading to increased adventitious rooting (Figure 1C). These interactions are summarized in Figure 3B.

ARF6 Positively Regulates Abundance and Cleavage of *ARF8* and *ARF17* Transcripts

When *ARF6* was overexpressed, the levels of *ARF8-T* and *ARF17-T* transcripts were increased (Figure 3C), whereas the

opposite effect was observed in *arf6-3* KO mutants (Figure 3C), indicating that *ARF6* positively regulates *ARF8* and *ARF17* total transcript abundance. By contrast, the levels of *ARF8-UC* and *ARF17-UC* decreased in the *ARF6-OX* line, indicating that *ARF6* promotes posttranscriptional degradation of *ARF8* and *ARF17* mRNA (Figure 3C). In addition, the level of *ARF6-UC* was much lower than the total transcript level, suggesting that a regulatory feedback mechanism activates the degradation of *ARF6* transcripts when the gene is overexpressed. The accumulation of *ARF17-UC* in *arf6-3* mutants provides further support for the hypothesis that *ARF6* activates *ARF17* mRNA cleavage. Interestingly, *ARF8-UC* does not accumulate in *arf6-3* mutants, as might be expected given the observed effects in the *ARF6-OX* line (Figure 3C). This can be explained by the observation that *ARF17*, when overexpressed, activates degradation of *ARF8* mRNA (Figure 3C). Therefore, increased cleavage of *ARF8* mRNA in *arf6-3* mutants is likely to be driven by the accumulation of *ARF17-UC* mRNA, resulting in *ARF17* overexpression and a consequent shift in the activator/repressor balance toward the repressor and a reduced number of adventitious roots in the *arf6-3* KO mutant (Figure 1C).

ARF8 Modulates *ARF* Transcript Abundance Including Posttranscriptional Regulation through the miRNA Pathway

In the *arf8-7* KO mutant (Figure 3C), *ARF6-T* levels were not affected, while those of *ARF17-T* increased, relative to the wild type, suggesting that *ARF8* negatively regulates *ARF17* transcript abundance, but not that of *ARF6*. The level of *ARF17-UC* showed a similar fold change to that of *ARF17-T*, indicating that the degradation of *ARF17* mRNA is unaffected in the *arf8-7* mutant. These findings suggest that *ARF8* does not regulate the posttranscriptional degradation of *ARF17* by *miR160*. In addition, the level of *ARF17-T* was not affected in the *ARF8-OX* line (Figure 3C), confirming that *ARF8* negatively regulates *ARF17* transcript abundance. Indeed, despite an increased level of *ARF6-UC* transcripts, *ARF17* transcript abundance was not affected in the *ARF8-OX* line, the high level of *ARF8-UC* transcripts overriding the effect an increased level of *ARF6* might otherwise have had on *ARF17* expression (cf. ARF6-OX and ARF8-OX panels in Figure 3C).

A decrease in *ARF6-UC* transcript levels was observed in the *arf8-7* mutant, indicating that *ARF8* negatively regulates the posttranscriptional degradation of *ARF6* by *miR167*. This hypothesis was confirmed by the higher levels of *ARF6-UC* and *ARF8-UC* transcripts than *ARF6-T* and *ARF8-T* transcripts observed in the *ARF8-OX* line (Figure 3C).

ARF17 Negatively Regulates the Expression of Activator *ARF*s

The *ARF17-OX* line showed reduced levels of both *ARF6-T* and *ARF8-T* transcripts (Figure 3C), in accordance with the reduced adventitious rooting observed in this line. However, the reduction of *ARF8* transcript abundance in *ARF17-OX* is likely to be a consequence of its lower levels of *ARF6-UC* transcripts, as observed in the *arf6-3* line, which completely lacks *ARF6* (Figure 3C). Indeed, in the *arf6-3* line, the downregulation of *ARF8* transcript level was even more dramatic and unlikely to be solely due to *ARF17* since *ARF17-UC* mRNA levels were only twofold increased (Figure 3C), while they were 14-fold higher than wild-type levels in the *ARF17-OX* line (Figure 3C). These findings indicate that *ARF6* plays a dominant role in the regulation of *ARF8* transcript level.

Since increased degradation of *ARF6* and *ARF8* mRNAs and accumulation of *ARF17-UC* mRNA appear to occur in *ARF17-OX* (Figure 3C), we suggest that *ARF17* positively regulates *ARF6* and *ARF8* posttranscriptional degradation by *miR167*, whereas it represses its own posttranscriptional degradation by *miR160*.

Posttranscriptional Regulation of *miR160* and *miR167* Homeostasis

Plant miRNAs are 20- to 24-nucleotide RNAs, which derive from primary miRNAs (pri-miRNAs) that are mostly transcribed by RNA polymerase II from regions located between protein-coding genes. The pri-miRNAs are then converted to stem-loop pre-miRNAs. This reaction is driven by the action of the C2H2-zinc finger protein SERRATE (SE; At2g27100), the double-stranded RNA binding protein HYPONASTIC LEAVES1 (HYL1; At1g09700), Dicer-like 1 (DCL1; At1g01040), and nuclear cap binding complex. Pre-miRNAs, or mature miRNAs produced by DCL1, are then exported to the cytoplasm possibly through the action of the HASTY protein (HST1; At3g05040) and other unknown factors. Mature RNA duplexes excised from pre-miRNAs are methylated by HUA ENHANCER1 (HEN1; At4g20910), a reaction that protects them from being degraded by the SMALL RNA DEGRADING NUCLEASE (SDN; At3g50100) class of exonucleases. The guide miRNA strand is then incorporated into AGO1 protein to carry out the cleavage of target mRNAs (Figure 4; reviewed in Voinnet, 2009). To gain further insights into the effects of *ARF* genes in the posttranscriptional regulation of the homeostasis of their respective regulatory microRNAs, we analyzed the steady state levels of the three pri-miR160 RNA precursors (*pri-miR160a*, *pri-miR160b*, and *pri-miR160c*) of *miR160*, which drives the degradation of *ARF17* transcripts, in the wild-type and mutant lines using real-time RT-PCR (Figure 5A). Similar analyses were also performed on the four pri-miR167 precursors (*pri-miR167a*, *pri-miR167b*, *pri-miR167c*, and *pri-miR167d*) of *miR167a*/*b*, *miR167c*, and *miR167d*, which target *ARF6* and *ARF8* transcripts for degradation (Figure 5A). In addition, we analyzed the steady state levels of the mature miRNAs *miR160*, *miR167a*/*b*, *miR167c*, and *miR167d* (Figure 5B).

As expected, the levels of *pri-miR160c* and *miR160* were elevated in the *miR160c-OX* line (Figures 5A and 5B). Apart from this exception, the levels of *pri-miR160s* and *pri-miR167s* were not different from wild-type levels in any of the lines analyzed, suggesting that none of the *ARFs* regulates the abundance of primary transcripts of either *MIR160* or *MIR167* genes (Figure 5A). Similarly, the level of mature miRNAs was not modified in the *arf10-3*, *arf16-3*, and *arf10-3 arf16-3* single and double mutant, suggesting that neither *ARF10* nor *ARF16* regulate posttranscriptional accumulation of *miR160* and *miR167s* (Figure 5B). By contrast, levels of mature *miR160* and *miR167s* were different from wild-type levels in the other mutant lines (Figure 5B) and were correlated with the cleavage of *ARF* transcripts (Figure 3C).

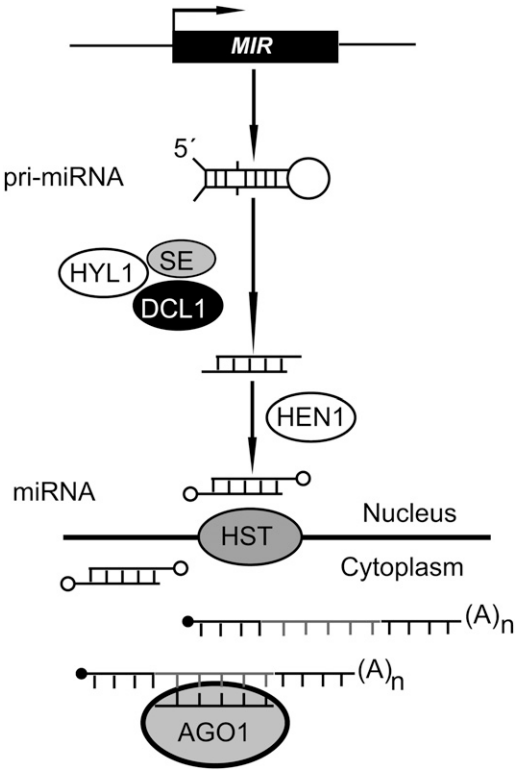

Figure 4. Schematic of the miRNA Maturation Process That Leads to the Cleavage of Target mRNAs.

pri-miRNAs are mostly transcribed by RNA polymerase II from miRNA encoding genes. The pri-miRNAs are processed into mature miRNAs through a reaction driven by the action of the C2H2-zinc finger protein SE, the double-stranded RNA binding protein HYL1, DCL1, and nuclear cap binding complex. Mature RNA duplexes excised from pre-miRNAs are methylated by HEN1 and exported to the cytoplasm possibly through the action of the HST1 protein. The guide miRNA strand is then incorporated into AGO1 protein to carry out the cleavage of target mRNAs.

More specifically, increased levels of mature *miR167s* were found in *ARF6-OX*, *ARF17-OX*, *arf6-3*, and *arf8-7* plants, in which the degradation of *ARF6* and *ARF8* transcripts is increased (Figure 3C), while reduced levels of mature *miR167s* compared with the wild type were found in *ARF8-OX* plants, in which *ARF6* and *ARF8* transcript degradation is reduced (Figure 3C). In the *ARF6-OX* and *ARF8-OX* lines, the increased *ARF17* transcript degradation can be explained by the increased level of mature *miR160* (Figures 3C and 5B). In the *arf6-3* and *ARF17-OX* lines, the reduced amount of mature *miR160* (Figure 5B) may explain the decrease in *ARF17* transcript degradation (Figure 3C), whereas in *arf8-7*, the degradation of *ARF17* transcripts is not affected (Figure 3C), which correlates with its wild-type level of mature *miR160* (Figure 5B). These results suggest that *ARF6*, *ARF8*, and *ARF17* regulate their own posttranscriptional mRNA degradation by modulating the amounts, and thus activities, of their associated microRNAs.

To date, only a few genes, *DCL1*, *HYL1*, *HEN1*, and *SE* (reviewed in Voinnet, 2009; Figure 4), have been shown to be involved in the miRNA maturation process in plants. We checked the expression of these genes in each of the *ARF* lines and did not find any significant variation compared with the wild type (Figures 5C and 5E). *DCL1* is regulated by a miRNA, *miR162*, so we checked the amount of both the total and uncleaved *DCL1* mRNAs. In both cases, there was no significant difference between any of the mutant lines and the wild type (Figure 5C). Furthermore, although it has been suggested that *DCL1* is the only *DCL* that processes miRNAs (Gasciolli et al., 2005), we also checked the expression of *DCL2* (At3g03300), *DCL3* (At3g43920), and *DCL4* (At5g20320) and did not detect any differences in their expression between the mutant and wild-type lines (see Supplemental Figure 4A online). Similarly, no variation was observed in the levels of either *pri-miR162* or mature *miR162*, which targets *DCL1* mRNA for degradation (Xie et al., 2004; Gasciolli et al., 2005) (Figure 5D). In addition, neither the expression level of *AGO1* and *HST1* nor the amount of the *pri-miR168a* (At4g19395) and *b* (At5g45307) or mature *miR168* that targets *AGO1* (At1g48410) were altered in any of the mutant lines (Figures 5C to 5E). These results show that although the amounts of *miR160* and *miR167* are modified in the *ARF* mutant lines, the main biogenesis pathway does not seem to be affected at the transcriptional level, suggesting the presence of further, as yet unknown, regulators that could specifically affect miRNA species. The findings that *miR160* and *miR167s* are differentially regulated in certain lines (i.e., the *ARF8-OX*, *ARF17-OX*, and *arf6-3* lines; Figure 5B) support this hypothesis.

DISCUSSION

Adventitious rooting is a complex trait that is affected by multiple factors and that displays a strong phenotypic plasticity. Hence, its regulation is likely to be finely tuned. Studies of *Arabidopsis* mutants with altered adventitious rooting parameters have allowed us to identify several candidate regulatory genes, including the auxin response factor *ARF17* (Sorin et al., 2005, 2006). Here, we confirm that *ARF17* is a negative regulator of adventitious root formation that could potentially integrate auxin and light signaling pathways affecting this process. We show that the balance between the negative regulator *ARF17* and positive regulators *ARF6* and *ARF8* as well as the maintenance of the homeostasis of their regulatory miRNAs plays a critical role in adventitious root formation. *ARF6* and *ARF8* have been previously reported to play interactive roles in the control of flower development (Nagpal et al., 2005). In the cited study, double mutants displayed stronger phenotypic divergence from wild-type counterparts than either of the single mutants and gene dosage effects were observed, such that *ARF6*/*arf6arf8*/*arf8* and *arf6*/*arf6arf8*/*ARF8* sesquimutants (i.e., homozygous for one mutation and hemizygous for the other) showed intermediate phenotypes between single and double mutants (Nagpal et al., 2005).

Here, we show that *ARF6* and *ARF8* also have similar dosage-dependent functions during adventitious root formation. Moreover, the ratio between the levels of uncleaved *ARF6* + *ARF8* (positive regulators) and *ARF17* (negative regulator) seems to be a key determinant of the number of adventitious roots induced. In

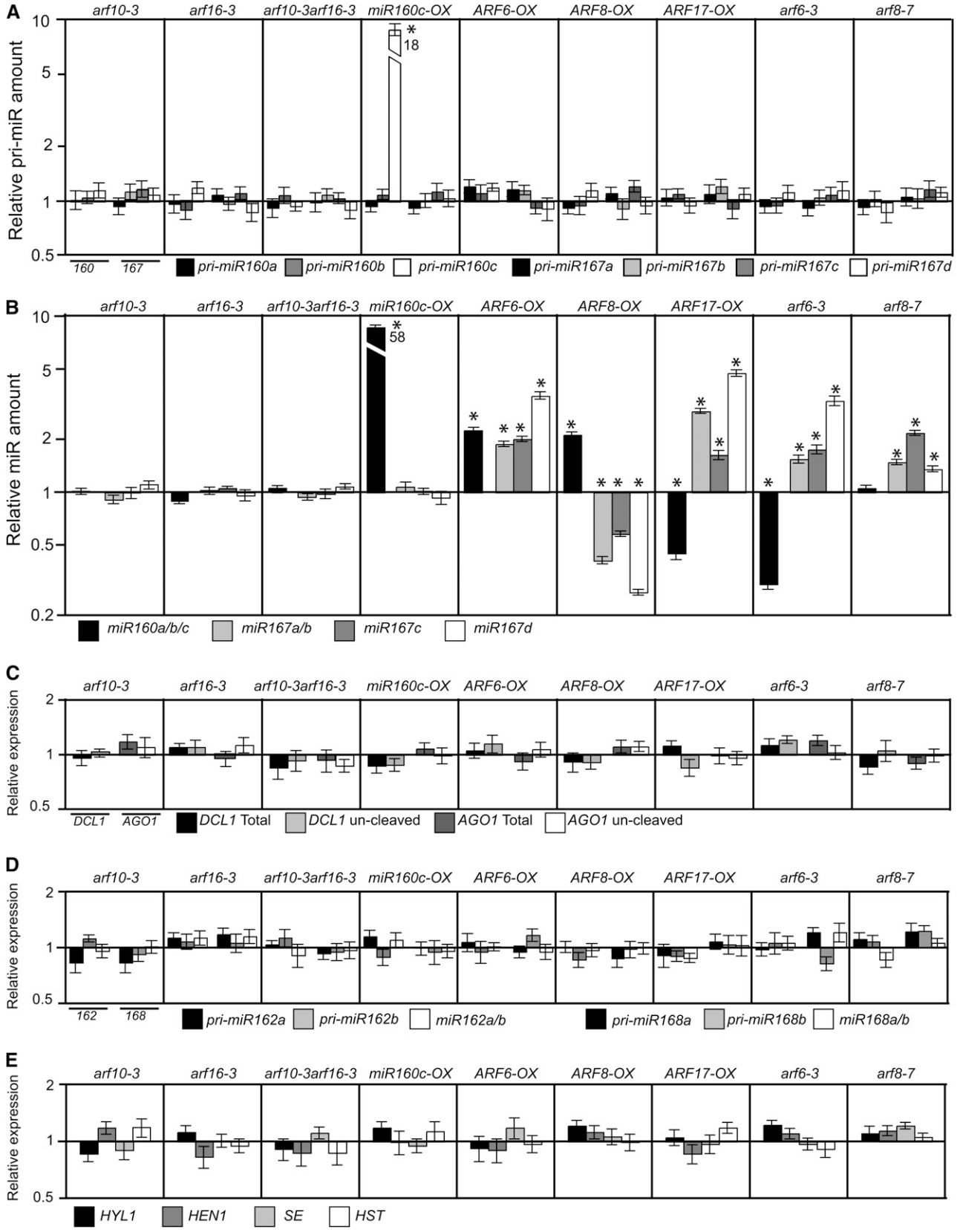

Figure 5. Real-Time RT-PCR Assessment of Posttranscriptional Regulation of *miR160* and *miR167* by *ARF6*, *ARF8*, and *ARF17*.

addition, we show that *ARF6* and *ARF8* expression patterns overlap in young seedlings, as they do in flowers (Nagpal et al., 2005), and that both are regulated by light. Nevertheless, since *ARF6* regulates *ARF8* transcript abundance, we suggest that light induction of *ARF8* may be driven by *ARF6*. The complexity of the interaction is emphasized by the finding that *ARF6* and *ARF8* have opposite effects on *ARF17* transcript abundance; *ARF8* negatively regulates *ARF17* transcript abundance, whereas *ARF6* is a positive regulator. In return, *ARF17* represses the transcript abundance of *ARF6* but has no effect on that of *ARF8*.

A model summarizing these probable interactions is shown in Figure 6, but the processes are likely to be more complex than the model indicates. In gel shift experiments we performed using different combinations of ARF6, ARF8, and ARF17 proteins with corresponding *ARF* promoter sequences, we found no evidence of any direct binding. The promoters of *ARF6*, *ARF8*, and *ARF17* contain one, one, and no consensus auxin response elements, respectively, and one, two, and four nonconsensus ones, respectively (see Supplemental Figure 5 online) that would be required for regulation by other ARFs (Guilfoyle, 2007). The gel shift experiments may not reflect the in vivo situation, but they leave open the possibility that *ARF6*, *ARF8*, and *ARF17* may indirectly regulate each other's transcription through as yet unknown intermediate transcription factors. In addition, although the effect of variations in *ARF* transcript levels is supported by a phenotype, the transcript abundance might not necessarily reflect the ARF protein abundance, suggesting that additional levels of regulation might exist.

ARF7 (At5g20730) and *ARF19* (At1g19220), which are involved in the regulation of both lateral and adventitious root development (Okushima et al., 2005; Wilmoth et al., 2005), are unlikely to be part of this network since their expression was not affected in any of the mutant lines analyzed here (see Supplemental Figure 4B online). This suggests that these two genes are not involved in regulatory pathways specific to adventitious root initiation but most likely involved in independent and/or downstream regulatory mechanisms common to lateral and adventitious root development.

ARF6, *ARF8*, and *ARF17* are also regulated at the posttranscriptional level by the miRNAs *miR167* and *miR160* (Mallory et al., 2005; Wu et al., 2006). We show here that the maintenance of *ARF6*, *ARF8*, and *ARF17* transcript homeostasis requires additional levels of posttranscriptional regulation. More specifically, we demonstrate that *ARF6* positively regulates the amounts of both *miR160* and *miR167s* at the posttranscriptional level, *ARF8* negatively regulates levels of *miR167*, while *ARF17* negatively regulates those of its own miRNA *miR160* but has a positive effect on the levels of *miR167s.* In principle, any step during the maturation process of miRNAs could be regulated. However, the core enzymes are widely expressed and no posttranslational regulation of the proteins involved in the process has been reported. In plants, two cases of feedback loops have been previously reported in which the expression of miRNAs is regulated by target genes (*DCL1* and *AGO1*, both of which are

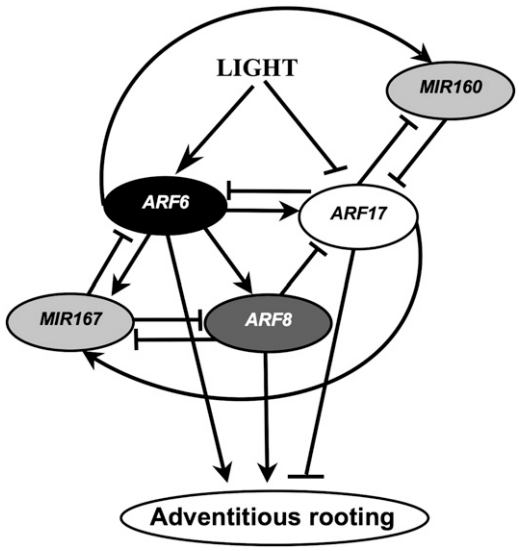

Figure 6. A Model Integrating the Regulatory Loops between *ARF* and *miRNA* Genes in the Control of Adventitious Rooting Based on Results Obtained in This Study.

Adventitious root initiation is controlled by a subtle balance of activator and repressor *ARF* transcripts, which is maintained by a complex regulatory network. *ARF6* has both a positive and a negative effect on *ARF8* and *ARF17* transcript levels. It regulates positively *ARF8* and *ARF17* total transcript levels, whereas it has a negative effect on their uncleaved transcript amount by modulating positively *miR160* and *miR167s* abundance, which drives degradation of *ARF17* and *ARF8* transcripts, respectively. By regulating miR167s, it also regulates its own uncleaved transcript level. Moreover, *ARF8* regulates negatively both *ARF17* total transcript amount and *miR167s* abundance and by consequence *ARF6* and its own uncleaved transcript level. In turn, *ARF17* represses *ARF6* total transcript abundance. In addition, *ARF17* regulates positively the pool of *miR167s* and thereby has a negative effect on *ARF6* and *ARF8* uncleaved transcript abundance. *ARF17* regulates its own uncleaved transcript abundance by feedback regulation of *miR160* level. *ARF6* and *ARF8* are positively regulated by light. Nevertheless, since *ARF6* regulates *ARF8* transcript abundance, we suggest that light induction of *ARF8* may be driven by *ARF6*. *ARF17* is repressed by light.

Figure 5. (continued).

Steady state levels of pri-miRNAs (pri-miR) (**[A]** and **[D]**) and mature miRNAs (**[B]** and **[D]**) were quantified in the hypocotyls of representative *ARF* mutant or overexpressing lines etiolated and transferred to the light for 72 h, as were *DCL1* and *AGO1* transcripts **(C)**. Steady state levels of *HYL1*, *HEN1*, *SE*, and *HST1* were quantified in the same conditions **(E)**. Gene expression values shown are relative to the expression in the wild type, for which the value is set to 1. Error bars indicate ± SE obtained from three independent RT-PCR experiments. A one-way ANOVA combined with the Dunnett's comparison test indicated that the values marked with an asterisk were significantly different from the wild-type value ($P < 0.01$; $n = 3$). All quantifications were repeated using two additional independent biological replicates and gave similar results.

involved in the miRNA biogenesis pathway; Mallory and Vaucheret, 2006). Posttranscriptional regulation of miRNA abundance has only been previously described in animal cells (Mineno et al., 2006; Obernosterer et al., 2006; Thomson et al., 2006; Wulczyn et al., 2007; Viswanathan et al., 2008), but here we uncover a new form of feedback regulation that does not affect the transcript abundance of *pri-miRNAs* but rather the levels of mature miRNA species. The regulation is mediated by modifications in the expression of the targeted transcripts, in these cases *ARF6*, *ARF8*, and *ARF17*. These findings suggest either that they act on the posttranscriptional regulatory steps during the processing of the pri-miRNAs or on the degradation/titration of the mature miRNAs. A family of exoribonucleases involved in the degradation of mature miRNAs was recently identified. These are encoded by the *SDN* genes in *Arabidopsis* and play a crucial role in the turnover of miRNAs (Ramachandran and Chen, 2008). Whether their expression is feedback regulated by miRNA-targeted genes still has to be investigated. At this point, we cannot exclude the possibility that the modulation of *miR160* and *miR167* levels in our ARF lines is due to a deregulation of *SDN* genes. Nevertheless, the observations that accumulation of *miR167s* is reduced and *miR160* increased in the *ARF8-OX* line and vice versa in the *ARF17-OX* and *arf6-3* KO mutants indicate that different regulatory mechanisms specifically affect the expression of *miR160* and *miR167* miRNAs. Interestingly, the noncoding gene *IPS1*, which contains a motif with sequence complementarity to miRNA *miR399*, was recently shown to be resistant to cleavage and to sequester miR399, thereby modulating its activity (Franco-Zorrilla et al., 2007). Similar mechanisms may exist for different miRNAs.

In conclusion, our results provide indications of posttranscriptional regulatory mechanisms that are likely to affect specific miRNA species and contribute to fine-tuning the regulation of quantitative genetic traits, such as adventitious rooting.

METHODS

Plant Material and Growth Conditions

The *ARF17-OX1* line (SALK 062511) has been previously described (Sorin et al., 2005). *ARF17-OX2* is a *35S:ARF17* line, described by Mallory et al. (2005) and provided by A. Mallory (Cell Biology Laboratory, Institut National de la Recherche Agronomique, Versailles, France). Two *ARF8*-overproducing lines (*ARF8-OX 10-1* and *ARF8-OX 7-5*) and the knockout *arf8-1* line have been described by Tian et al. (2004) and were provided by K.T. Yamamoto (Division of Biological Sciences, Hokkaido University, Sapporo, Japan). We identified a knockout *arf8* mutant (*arf8-7*) in the GABI-Kat collection (line 510C01). The *ARF6* overexpressing line (*ARF6-OX*) (Nagpal et al., 2005) was provided by J.W. Reed (University of North Carolina at Chapel Hill, NC). We identified an *ARF6* knockout mutant (*arf6-3*) in the Versailles collection of T-DNA insertion lines (line EAV20, FST 219A05). Two *ARF10* knockout mutants (*arf10-3* and *arf10-4*) were identified in the GABI-Kat collection (lines 086F05 and 274H01, respectively), and an *ARF16* knockout mutant (*arf16-3*) was identified among the SALK insertion lines (SALK_021432). Lines *MIR160a-OX* and *MIR160c-OX*, respectively overexpressing genes *MIR160a* and *MIR160c* (Wang et al., 2005), were provided by X.Y. Chen (Institute of Plant Physiology and Ecology, Shanghai Institutes for Biological Sciences, Shanghai, China). *ARF8-OX 10-1*, *ARF8-OX 7-5*, *arf8-1*, and *arf6-3* are in Wassilewskija background; *arf8-7*, *ARF6-OX*, *ARF17-OX2*, *MIR160a-OX*, *MIR160c-OX*, *arf10-3*, and *arf10*-4 are in Col-0 background; while *arf16-3* and *ARF17-OX1* are in the Col-8 background. The primers used for genotyping each of the newly described mutant lines are listed in Supplemental Table 1 online.

Seeds were sterilized and sown in vitro as previously described (Sorin et al., 2005). Plates were incubated at 4°C for 48 h for stratification and transferred to the light for several hours to induce germination. They were then wrapped with three layers of aluminum foil and kept in the dark until the seedling hypocotyls reached an average length of 6 mm (~48 h). Seedlings were then transferred to the light for induction of adventitious roots. Adventitious roots and lateral roots were counted, and the primary root length measured 7 d after transfer to the light. For each biological replicate, at least 30 seedlings were analyzed, and each experiment was repeated at least three times. A one-way ANOVA combined with a Tukey's multiple comparison test was performed to analyze the differences between genotypes' mean and variance using the software GraphPad Prism version 5.0 for Mac.

The growth conditions were as follows: 16 h light (120 μmol m^{-2} s^{-1}, 20°C)/8 h dark (15°) cycles. For the monochromatic (blue, red, and far red) light experiments, seedlings from *promARF6:GUS*, *promARF8:GUS*, and *promARF17:GUS* lines were grown in the conditions described above until the hypocotyl reached an average length of 6 mm. The plants were then transferred to individual monochromatic cabinets in continuous light and constant temperature for an additional 72 h. Blue light (460 nm, 80 μmol m^{-2} s^{-1}, 24°C $\pm$ 2°C), red light (650 nm, 15 μmol m^{-2} s^{-1}, 22°C $\pm$ 2°C), and far-red light (750 nm, 13 μmol m^{-2} s^{-1}, 23°C $\pm$ 2°C).

Analysis of Promoter Activity

Arabidopsis thaliana lines expressing *promARF6:GUS*, *promARF8:GUS*, *promMIR167a:GUS*, *promMIR167b:GUS*, *promMIR167c:GUS*, and *promMIR167d:GUS* (Nagpal et al., 2005; Wu et al., 2006) were provided by J.W. Reed. A line expressing *promMIR160c:GUS* (Wang et al., 2005) was provided by X.Y. Chen. A 1473-bp-long fragment upstream from the start codon of the *ARF17* gene was amplified by applying PCR to genomic DNA (forward primer, 5′-AAGGATTAAAGTGGAAAAGGT-3′; reverse primer, 5′-AAACGAAGTCAGCGAATGAA-3′), cloned using a pENTR/D-TOPO Cloning Kit (Invitrogen), and transferred into the pKGWFS7 binary vector (Karimi et al., 2002) using a Gateway LR Clonase Enzyme Mix (Invitrogen) according to the manufacturer's instructions. Transgenic *Arabidopsis* plants expressing the *promARF17:GUS* fusion were generated by *Agrobacterium tumefaciens*–mediated floral dipping (Clough and Bent, 1998), and the expression pattern was checked in the T2 progeny of 15 independent transgenic lines. One representative homozygous line was used for further characterization. Histochemical assays of GUS expression were performed as previously described (Sorin et al., 2005).

RNA Isolation and cDNA Synthesis

Seeds from the *arf* mutants and *ARF* overexpressing lines were sown in vitro and germinated in the dark according to Sorin et al. (2005) until the hypocotyls of the germinating seedlings reached an average length of 6 mm. They were then transferred to the light for 72 h, and an average of 200 hypocotyls per sample were dissected, pooled, flash-frozen in liquid nitrogen, and ground into powder. Samples were prepared from three independent biological replicates. Total RNA was extracted and enriched in miRNA using a *miR*Vana miRNA isolation kit (Ambion) according to the manufacturer's instructions. Portions (10 μg) of the resulting RNA preparations were treated with DNaseI using a DNA*free* Kit (Ambion) and polyadenylated using poly(A) polymerase (Ambion) according to the manufacturer's instructions, then phenol:chloroform extracted, ethanol-precipitated, and dissolved in di-ethyl pyro-carbonate-treated deionized water. Modified cDNA was synthesized according to Thomson et al.

(2006) by reverse transcribing 10 μg of polyadenylated RNA using Superscript III reverse transcriptase (Invitrogen) with 2.5 μg of random hexamers and 500 ng of oligo(dT) adapter primer (5′-GCGAGCACA-GAATTAATACGACTCACTATAGGTTTTTTTTTTTTVN-3′) according to the manufacturer's instructions. The reaction was stopped by incubation at 70°C for 10 min, and the reaction mixture was then treated with RNaseH (Invitrogen) according to the manufacturer's instructions and diluted by adding 1 mL of deionized water. All cDNA samples were tested by PCR using specific primers flanking an intron sequence to confirm the absence of genomic DNA contamination.

Real-Time RT-PCR Experiment Design

ARF and *miRNA* transcript levels were assessed in three independent biological replicates by real-time RT-PCR (or quantitative RT-PCR), in assays with triplicate reaction mixtures (final volume, 20 μL) containing 5 μL of cDNA, 0.5 μM of both forward and reverse primers, and 1× FastStart SYBR Green Master mix (Roche). Real-time RT-PCR experiments used a balanced randomized block design, as recently advised (Rieu and Powers, 2009). An iCycler iQ real-time PCR detection system (Bio-Rad) (for data shown in Figures 3 and 4) and a LightCycler (Roche) (for data shown in Figures 2O to 2S) were used to acquire the CT values for each sample (i.e., the crossing threshold values, which are the number of PCR cycles required for the accumulated fluorescence signal to cross a threshold above the background). Steady state levels of uncleaved *ARF* transcripts were quantified using primers spanning the miRNA target site, and steady state levels of total transcripts were estimated using primers annealing to the 3′ end of the cDNAs (see Supplemental Figure 2B online). The following standard protocol was applied for the amplification of each of the *ARF* mRNAs: 10 min at 95°C, followed by 40 cycles of 10 s at 95°C, 15 s at 60°C, and 15 s at 72°C. For the pri-miRNA PCR, the same protocol was applied except the annealing temperature was 65°C. Mature miRNA (*miR*) was quantified according to the high-stringency protocol described by Shi and Chiang (2005), except the reverse primer 5′-GCGAGCACA-GAATTAATACGAC-3′ was used in conjunction with a sequence-specific primer to each miRNA as described by Thomson et al. (2006), which was lengthened by one (A) on the 3′ end to ensure the anchorage of the primer on the poly(T) of the mature miRNA cDNA and avoid its hybridization on the pri-miRNA cDNA (see Supplemental Figure 2A online).

Each amplicon was first sequenced to ensure the specificity of the amplified sequence and, in order to check that the fluorescence signal was derived from the single intended amplicon in the succeeding runs, a melting curve analysis was added to each PCR program and the size of PCR products was systematically assessed by electrophoresis in agarose gels (see Supplemental Figure 2C online). The primer sequences used for all target genes are presented in Supplemental Table 2 online.

Real-Time RT-PCR Data Analysis

Relative standard curves describing the PCR efficiencies (E) for each primer pair were generated for each amplicon according to Larionov et al. (2005). Normalization of real-time RT-PCR was performed using reference genes (R), which were selected and validated as follows. Eleven genes (see Supplemental Table 3 online for primer sequences) were chosen for their putative stability of expression according to Czechowski et al. (2005) and Gutierrez et al. (2008). Their expression in our experimental material (i.e., in hypocotyls from each of the lines grown under our experimental conditions) was then assessed, and they were ranked according to their stability of expression using geNorm software (Vandesompele et al., 2002). *APT1* and *TIP41* were the most stably expressed genes among the 11 tested and thus were used to normalize the real-time RT-PCR data. The normalized expression patterns obtained using both reference genes were similar, so only the data normalized with *APT1* are shown in this article.

In Figure 2, the expression in the wild type is calculated using the formula $E_R^{CT_{WT}}/E_T^{CT_{WT}}$ [i.e., $(1/E_T^{CT_{WT}})/(1/E_R^{CT_{WT}})$: the normalized relative quantity of template in the original sample], the expression levels of target genes being relative to those of the reference gene.

In Figures 3 and 4, CT and E values were used to calculate expression using the formula $E_T^{(CT_{WT}-CT_M)}/E_R^{(CT_{WT}-CT_M)}$, where (T) is the target gene and (R) the reference gene, CT is the crossing threshold value, (M) is related to cDNA from the mutant line and (WT) from wild type. In these figures, the data in mutants are presented as relative to the wild type, the calibrator.

All real-time RT-PCR results shown in Figures 2 to 4 are data of means and corresponding standard errors obtained for the first biological replicate, as calculated from the three technical replicates and using the method for calculation of standard errors in relative quantification recommended by Rieu and Powers (2009). A one-way ANOVA combined with a Dunnett's comparison test was performed to analyze the differences between genotypes' mean and the wild type using the software GraphPad Prism version 5.0 for Mac. Results obtained with the second and the third biological replicates displayed the same gene expression patterns as the ones shown in Figures 2 to 4.

Accession Numbers

Sequence data from this article can be found in the Arabidopsis Genome Initiative or GenBank/EMBL databases under the following accession numbers: *AGO1* (At1g48410), *APT1* (At1g27450), *ARF6* (At1g30330), *ARF7* (At5g20730), *ARF8* (At5g37020), *ARF10* (At2g28350), *ARF16* (At4g30080), *ARF17* (At1g77850), *ARF19* (At1g19220), *DCL1* (At1g01040), *DCL2* (At3g03300), *DCL3* (At3g43920), *DCL4* (At5g20320), *HEN1* (At4g20910), *HST1* (At3g05040), *HYL1* (At1g09700), *MIR160a* (At2g39175), *MIR160b* (At4g17788), *MIR160c* (At5g46845), *MIR162a* (At5g08185), *MIR162b* (At5g23065), *MIR167a* (At3g22886), *MIR167b* (At3g63375), *MIR167c* (At3g04765), *MIR167d* (At1g31173), *MIR168a* (At4g19395), *MIR168b* (At5g45307), *SE* (At2g27100), *SDN* (At3g50100), and *TIP41* (At4g34270).

Supplemental Data

The following materials are available in the online version of this article.

Supplemental Figure 1. Root Length and Lateral Root Number.

Supplemental Figure 2. Experimental Procedures Followed for the Different Real-Time RT-PCR Analyses.

Supplemental Figure 3. Expression Pattern of *promARF6:GUS*, *promARF8:GUS*, and *promARF17:GUS* under Different Light Conditions during the Early Stages of Adventitious Root Formation.

Supplemental Figure 4. Real-Time RT-PCR Assessment of the Transcript Level of *DCL2*, *DCL3*, *DCL4*, *ARF7*, and *ARF19.*

Supplemental Figure 5. Consensus and Nonconsensus AuxREs in the Promoter Sequence of *ARF6*, *ARF8*, and *ARF17.*

Supplemental Table 1. List of Specific Primers Used for Genotyping Newly Identified Mutant T-DNA Lines.

Supplemental Table 2. Sequences of Primers Used for Quantifying Target Genes by Real-Time RT-PCR.

Supplemental Table 3. Sequences of Primers for Candidate Reference Genes Tested by geNorm.

ACKNOWLEDGMENTS

We thank R. Bhalerao, M. Grebe, E. Sundberg, and H. Vaucheret for stimulating discussions and critical reading of the manuscript and

H. Demailly for technical assistance. We also thank the European Arabidopsis Stock Centre (NASC), the Centre des Ressources of Institut National de la Recherche Agronomique and the GABI-Kat stock center for providing seeds. We are grateful to A. Mallory (Institut National de la Recherche Agronomique), K.T. Yamamoto (Hokkaido University, Japan), J.W. Reed (University of North Carolina), and X.Y. Chen (Shanghai Institutes for Biological Sciences, Shanghai, China) for kindly providing various mutant or overexpressing lines. This work was supported by the Institut National de la Recherche Agronomique, the Swedish Natural Sciences Research Council, the Swedish Foundation for Strategic Research, and the C. Trygger foundation (C.B.).

Received December 2, 2008; revised September 3, 2009; accepted September 14, 2009; published October 9, 2009.

REFERENCES

Allen, E., Xie, Z., Gustafson, A.M., and Carrington, J.C. (2005). MicroRNA-directed phasing during trans-acting siRNA biogenesis in plants. Cell **121:** 207–221.

Clough, S.J., and Bent, A.F. (1998). Floral dip: A simplified method for Agrobacterium-mediated transformation of *Arabidopsis thaliana*. Plant J. **16:** 735–743.

Czechowski, T., Stitt, M., Altmann, T., Udvardi, M.K., and Scheible, W.R. (2005). Genome-wide identification and testing of superior reference genes for transcript normalization in Arabidopsis. Plant Physiol. **139:** 5–17.

Franco-Zorrilla, J.M., Valli, A., Todesco, M., Mateos, I., Puga, M.I., Rubio-Somoza, I., Leyva, A., Weigel, D., Garcia, J.A., and Paz-Ares, J. (2007). Target mimicry provides a new mechanism for regulation of microRNA activity. Nat. Genet. **39:** 1033–1037.

Gasciolli, V., Mallory, A.C., Bartel, D.P., and Vaucheret, H. (2005). Partially redundant functions of Arabidopsis DICER-like enzymes and a role for DCL4 in producing trans-acting siRNAs. Curr. Biol. **15:** 1494–1500.

Gifford, M.L., Dean, A., Gutierrez, R.A., Coruzzi, G.M., and Birnbaum, K.D. (2008). Cell-specific nitrogen responses mediate developmental plasticity. Proc. Natl. Acad. Sci. USA **105:** 803–808.

Guilfoyle, T. (2007). Plant biology: Sticking with auxin. Nature **446:** 621–622.

Guilfoyle, T.J., and Hagen, G. (2007). Auxin response factors. Curr. Opin. Plant Biol. **10:** 453–460.

Gutierrez, L., Mauriat, M., Guenin, S., Pelloux, J., Lefebvre, J.F., Louvet, R., Rusterucci, C., Moritz, T., Guerineau, F., Bellini, C., and Van Wuytswinkel, O. (2008). The lack of a systematic validation of reference genes: a serious pitfall undervalued in reverse transcription-polymerase chain reaction (RT-PCR) analysis in plants. Plant Biotechnol. J. **6:** 609–618.

Inukai, Y., Sakamoto, T., Ueguchi-Tanaka, M., Shibata, Y., Gomi, K., Umemura, I., Hasegawa, Y., Ashikari, M., Kitano, H., and Matsuoka, M. (2005). Crown rootless1, which is essential for crown root formation in rice, is a target of an AUXIN RESPONSE FACTOR in auxin signaling. Plant Cell **17:** 1387–1396.

Karimi, M., Inze, D., and Depicker, A. (2002). GATEWAY vectors for Agrobacterium-mediated plant transformation. Trends Plant Sci. **7:** 193–195.

Larionov, A., Krause, A., and Miller, W. (2005). A standard curve based method for relative real time PCR data processing. BMC Bioinformatics **6:** 62.

Liu, H.J., Wang, S.F., Yu, X.B., Yu, J., He, X.W., Zhang, S.L., Shou, H.X., and Wu, P. (2005). ARL1, a LOB-domain protein required for adventitious root formation in rice. Plant J. **43:** 47–56.

Mallory, A.C., Bartel, D.P., and Bartel, B. (2005). MicroRNA-directed regulation of *Arabidopsis* AUXIN RESPONSE FACTOR17 is essential for proper development and modulates expression of early auxin response genes. Plant Cell **17:** 1360–1375.

Mallory, A.C., and Vaucheret, H. (2006). Functions of microRNAs and related small RNAs in plants. Nat. Genet. **38**(Suppl): S31–S36.

Mineno, J., Okamoto, S., Ando, T., Sato, M., Chono, H., Izu, H., Takayama, M., Asada, K., Mirochnitchenko, O., Inouye, M., and Kato, I. (2006). The expression profile of microRNAs in mouse embryos. Nucleic Acids Res. **34:** 1765–1771.

Nagpal, P., Ellis, C.M., Weber, H., Ploense, S.E., Barkawi, L.S., Guilfoyle, T.J., Hagen, G., Alonso, J.M., Cohen, J.D., Farmer, E.E., Ecker, J.R., and Reed, J.W. (2005). Auxin response factors ARF6 and ARF8 promote jasmonic acid production and flower maturation. Development **132:** 4107–4118.

Obernosterer, G., Leuschner, P.J., Alenius, M., and Martinez, J. (2006). Post-transcriptional regulation of microRNA expression. RNA **12:** 1161–1167.

Okushima, Y., et al. (2005). Functional genomic analysis of the AUXIN RESPONSE FACTOR gene family members in *Arabidopsis thaliana*: Unique and overlapping functions of ARF7 and ARF19. Plant Cell **17:** 444–463.

Ramachandran, V., and Chen, X. (2008). Degradation of microRNAs by a family of exoribonucleases in Arabidopsis. Science **321:** 1490–1492.

Rhoades, M.W., Reinhart, B.J., Lim, L.P., Burge, C.B., Bartel, B., and Bartel, D.P. (2002). Prediction of plant microRNA targets. Cell **110:** 513–520.

Rieu, I., and Powers, S.J. (2009). Real-time quantitative RT-PCR: Design, calculations, and statistics. Plant Cell **21:** 1031–1033.

Shi, R., and Chiang, V.L. (2005). Facile means for quantifying microRNA expression by real-time PCR. Biotechniques **39:** 519–525.

Sorin, C., Bussell, J.D., Camus, I., Ljung, K., Kowalczyk, M., Geiss, G., McKhann, H., Garcion, C., Vaucheret, H., Sandberg, G., and Bellini, C. (2005). Auxin and light control of adventitious rooting in *Arabidopsis* require ARGONAUTE1. Plant Cell **17:** 1343–1359.

Sorin, C., Negroni, L., Balliau, T., Corti, H., Jacquemot, M.P., Davanture, M., Sandberg, G., Zivy, M., and Bellini, C. (2006). Proteomic analysis of different mutant genotypes of Arabidopsis led to the identification of 11 proteins correlating with adventitious root development. Plant Physiol. **140:** 349–364.

Thomson, J.M., Newman, M., Parker, J.S., Morin-Kensicki, E.M., Wright, T., and Hammond, S.M. (2006). Extensive post-transcriptional regulation of microRNAs and its implications for cancer. Genes Dev. **20:** 2202–2207.

Tian, C.E., Muto, H., Higuchi, K., Matamura, T., Tatematsu, K., Koshiba, T., and Yamamoto, K.T. (2004). Disruption and overexpression of auxin response factor 8 gene of Arabidopsis affect hypocotyl elongation and root growth habit, indicating its possible involvement in auxin homeostasis in light condition. Plant J. **40:** 333–343.

Vandesompele, J., De Preter, K., Pattyn, F., Poppe, B., Van Roy, N., De Paepe, A., and Speleman, F. (2002). Accurate normalization of real-time quantitative RT-PCR data by geometric averaging of multiple internal control genes. Genome Biol. **3:** RESEARCH0034.

Viswanathan, S.R., Daley, G.Q., and Gregory, R.I. (2008). Selective blockade of microRNA processing by Lin28. Science **320:** 97–100.

Voinnet, O. (2009). Origin, biogenesis, and activity of plant microRNAs. Cell **136:** 669–687.

Wang, J.W., Wang, L.J., Mao, Y.B., Cai, W.J., Xue, H.W., and Chen, X.Y. (2005). Control of root cap formation by microRNA-targeted auxin response factors in *Arabidopsis*. Plant Cell **17:** 2204–2216.

Williams, L., Carles, C.C., Osmont, K.S., and Fletcher, J.C. (2005). A database analysis method identifies an endogenous trans-acting short-interfering RNA that targets the Arabidopsis ARF2, ARF3, and ARF4 genes. Proc. Natl. Acad. Sci. USA **102:** 9703–9708.

Wilmoth, J.C., Wang, S., Tiwari, S.B., Joshi, A.D., Hagen, G., Guilfoyle, T.J., Alonso, J.M., Ecker, J.R., and Reed, J.W. (2005). NPH4/ARF7 and ARF19 promote leaf expansion and auxin-induced lateral root formation. Plant J. **43:** 118–130.

Wu, M.F., Tian, Q., and Reed, J.W. (2006). Arabidopsis microRNA167 controls patterns of ARF6 and ARF8 expression, and regulates both female and male reproduction. Development **133:** 4211–4218.

Wulczyn, F.G., Smirnova, L., Rybak, A., Brandt, C., Kwidzinski, E., Ninnemann, O., Strehle, M., Seiler, A., Schumacher, S., and Nitsch, R. (2007). Post-transcriptional regulation of the let-7 microRNA during neural cell specification. FASEB J. **21:** 415–426.

Xie, Z., Johansen, L.K., Gustafson, A.M., Kasschau, K.D., Lellis, A. D., Zilberman, D., Jacobsen, S.E., and Carrington, J.C. (2004). Genetic and functional diversification of small RNA pathways in plants. PLoS Biol. **2:** E104.